The Effect of Dust Radiative Heating on Low-Level Frontogenesis

SHOU-JUN CHEN* AND YING-HWA KUO

National Center for Atmospheric Research,† Boulder, Colorado

WEI MING AND HONG YING

Department of Geophysics, Peking University, Beijing, China

(Manuscript received 29 March 1994, in final form 7 October 1994)

ABSTRACT

Severe dust storms frequently occur over northwestern China during spring. They are often associated with strong fronts. In this paper, numerical simulations are performed to examine the effect of dust radiative heating on surface frontogenesis.

The absorption and multiple scattering of the dust are included in an atmospheric radiation scheme. A two-dimensional primitive equation model with 20 levels in the vertical is used for idealized simulations. After a 12-h integration, a strong narrow front zone is created below 650 mb. The horizontal potential temperature gradient reaches 6 K $(100\ \text{km})^{-1}$, which is three times as large as that in the initial data. A direct vertical transverse circulation is established along the frontal zone, which is qualitatively similar to the observations.

The results show positive interaction between low-level frontogenesis and dust radiative heating. The adiabatic frontogenesis forcing is enhanced by the feedback of the dust radiative heating. These results suggest that the dust heating can significantly affect mesoscale weather systems in arid and desert regions.

1. Introduction

Severe dust storms occur frequently over arid and desert regions in northwestern China during spring (Chen and Chen 1987). They often occur together with strong surface fronts. Large amounts of airborne dust associated with gale-force winds can restrict visibility quite severely. The horizontal visibility can drop below 50 m, and the sky becomes totally dark at noon. This is called the "black wind" in China. Heavy dust and sand transport causes severe damage to agriculture and desertification of the surrounding area. Large amounts of soil dust can be transported to as far east as the tropical North Pacific (Duce et al. 1980; Shaw 1980).

The dust storm of April 1977 over northwestern China has been studied by Xu et al. (1979). The dust storm was associated with a strong surface front. Figure 1a shows the 850-mb map for this case. Because the average surface height in this area is near 1500 m, the 850-mb analysis represents the surface analysis. A strong front between the cold anticyclone and the warm trough is evident. The horizontal temperature gradient reached 10°C $(100\ \text{km})^{-1}$. As this front passed Zhangye by 1800 LST, the temperature dropped 6.8°C in 10 min, showing the mesoscale structure of the front. The dust storm extended 400 km from behind the front with a vertical depth of near 4 km. The vertical cross section perpendicular to the front (Fig. 1b) showed that the front extended to 700 mb. The convergence in the surface frontal region reached $-9 \times 10^{-5}\ \text{s}^{-1}$. Above 650 mb, the airflow was divergent. Strong upward motion occurred over and ahead of the surface front with a maximum near 650 mb. Downward motion occurred behind the front. This indicates a thermally direct vertical circulation associated with the front.

Xu et al. (1979) pointed out that this front had its greatest intensity during the day and weakened at night. It is hypothesized that the feedback of dust radiative heating plays a role in the surface frontogenesis. First, the dust radiative heating affects the surface temperature. In the daytime, the air is very dry and there is no cloud ahead the front. Strong solar radiative heating increases the surface temperature as well as the surface sensible heat flux. Behind the front, the presence of dust may result in a relative surface cooling owing to radiative flux divergence. Thus, the surface temperature contrast is enhanced in the frontal zone. Second, in the lower troposphere, where the dust concentrated behind the front, the atmosphere is heated due to the direct absorption and multiple scattering of solar radiation by the dust. This may result in an increase in upward mo-

* Permanent affiliation: Department of Geophysics, Peking University, Beijing, China.

† The National Center for Atmospheric Research is sponsored by the National Science Foundation.

Corresponding author address: Dr. Shou-Jun Chen, Dept. of Geophysics, Peking University, Beijing 100871, China.

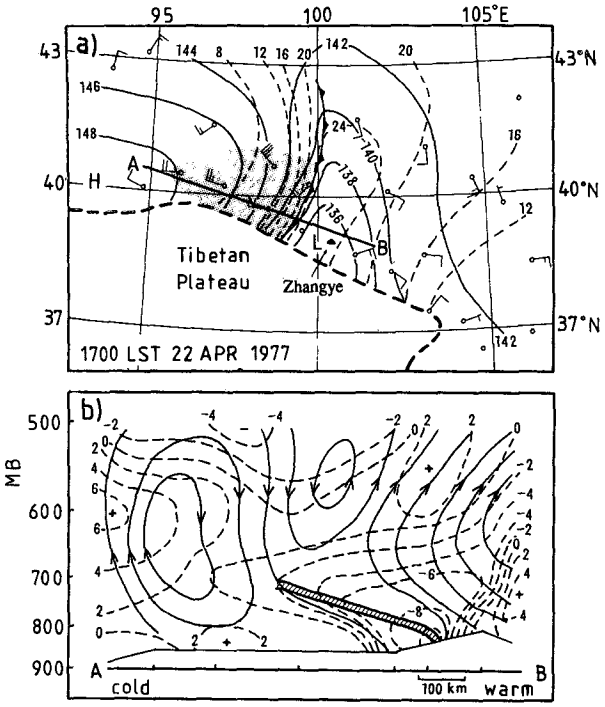

FIG. 1. (a) The 850-mb analysis for 22 April 1977. Solid lines are height contours in 10 gpm; dashed lines are isotherms (°C). The dust storm area is shaded. Heavy line AB indicates the location of the cross section. (b) The vertical cross section through the dust storm area. Double line with hatched areas indicates the front; dashed lines are divergence (10^{-5} s^{-1}), and solid lines with arrows show the vertical circulation (from Xu et al. 1979).

tion and surface convergence, which can be seen in Fig. 1b. Strong low-level convergence can, in turn, intensify surface frontogenesis.

In this paper, idealized numerical simulations are performed using a two-dimensional model with dust radiative heating. The objective is to examine the effect of dust heating on the intensity of the low-level front.

2. Mesoscale model and experiment design

A two-dimensional primitive equation model in σ coordinate with 20 levels in the vertical is used for the simulation. The framework of the model is similar to that of Anthes and Warner (1978). The horizontal grid spacing is 50 km.

Energy-conserving schemes for horizontal and vertical advection (Arakawa and Lamb 1981; Suarez and Arakawa 1979) are used. Since the dust storm was very dry, with no precipitation, the moisture processes are not included in the model. The surface heat flux is calculated by a bulk aerodynamic method. The lateral boundary condition developed by Hack and Schubert (1981) is used, which allows gravity waves generated in the model to propagate through the boundary.

The dust radiative heating scheme in the model is presented in the appendix. Figure 2a shows the distribution of the extinction coefficient used in this study, which is specified based on lidar observations taken in Beijing for a severe dust storm at 1600 LST 5 May 1982 (Qiu et al. 1984). The area enclosed by a contour of 0.5 km^{-1} can be regarded as the region occupied by the dust. The horizontal extent of the dust varies from 150 to 600 km, and the vertical extent reaches 800 mb. For simplicity, it is assumed that the distribution of the dust does not change with time; this implies that there is no dust life cycle in the model. However, because the shortwave radiation varies with the solar zenith angle, there is a diurnal variation in the dust radiative heating rate in the model.

To calculate the solar angle, the latitude is chosen as 45°, the declination of the sun is 23.5° (the summer solstice), and the initial hour angle is $-\pi/2$, which is equivalent to 0600 LST. Therefore, the 12-h integration represents the 1800 LST results.

The instantaneous maximum heating reaches 20 K day^{-1} and occurs near the top of the dust region, where the multiple scattering and absorption of the solar radiation are large (Fig. 2b). Carlson and Benjamin (1980) got the maximum heating greater than 10°C day^{-1} for the Saharan dust. Considering that the turbidity of the "black wind" is larger than that of Sa-

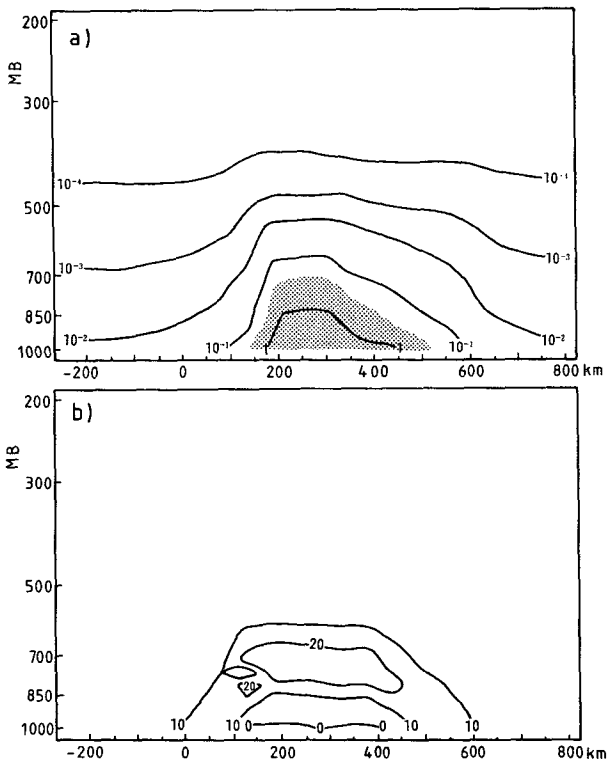

FIG. 2. (a) The idealized distribution of the extinction coefficient in the model simulation (km^{-1}). Striped area denotes the dust region. (b) The maximum instantaneous dust heating calculated by using the radiative scheme in the appendix (°C day^{-1}).

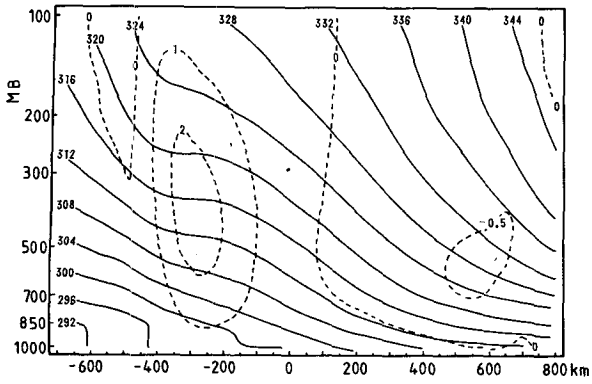

FIG. 3. The initial value for the simulation. Solid lines are potential temperature (K), dashed lines are vertical velocity (μb s^{-1}).

haran dust and the date we used is solstice, which has the strongest solar radiation, this heating rate represents the upper bound of dust radiative heating effect.

We specified a temperature field with an initial north–south temperature gradient of 2 K (100 km)$^{-1}$ and a constant lapse rate of 6 K km^{-1}. The wind field is calculated from the thermal wind equation. The model is integrated for 6 h without dust heating to get a nearly balanced wind and mass fields, which then serve as the initial conditions (hour 0) for the subsequent experiments. As shown in Fig. 3, a weak front is located at near 450 km and is associated with a weak direct vertical circulation. The horizontal temperature gradient has increased to 3 K (100 km)$^{-1}$.

Two experiments are performed: one with dust heating, referred to as DRH, and the other without dust heating, referred to as CON. By comparing the differences between these two experiments, the effects of dust heating on the low-level frontogenesis can be evaluated.

3. Results

Figure 4a shows the distribution of potential temperature and vertical velocity after a 12-h integration (1800 LST) in DRH. A strong and narrow frontal zone is created in the lower troposphere. The horizontal gradient at the surface reaches 6 K (100 km)$^{-1}$ (Fig. 4c), which is twice as large as that in the initial field shown in Fig. 3. The front, defined by the maximum potential temperature gradient, extends up to 650 mb and has a

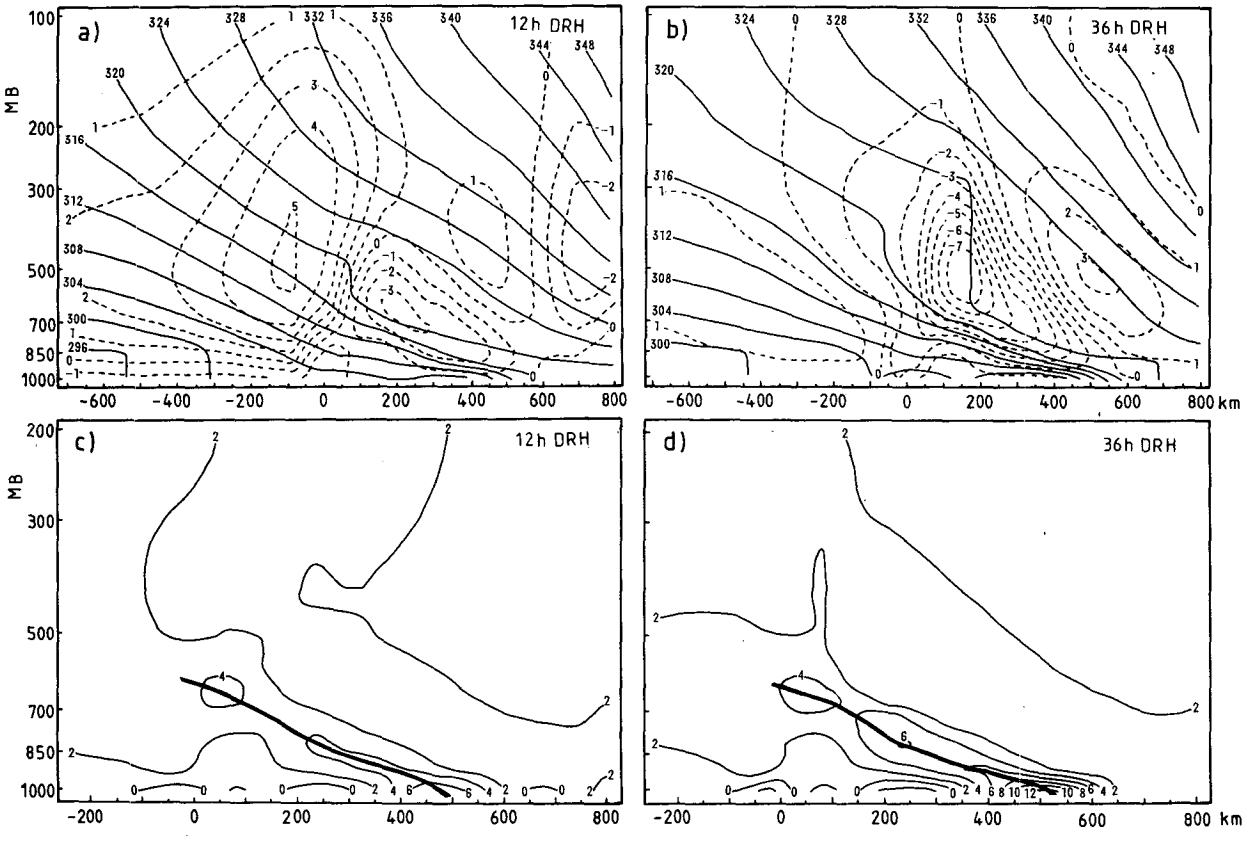

FIG. 4. (a) The 12-h simulated potential temperature [solid lines, (K)] and vertical velocity [dashed lines (μb s^{-1})] in DRH. (b) Same as in (a) but for a 36-h simulation. (c) The 12-h simulated horizontal potential temperature gradient in DRH, [K (100 km)$^{-1}$]. Thick solid line indicates the axis of maximum potential temperature gradient. (d) Same as in (c) but for a 36-h simulation.

slope of nearly $1/100$. Strong upward motions occur over the surface front with a maximum -3 μb s^{-1} at 650 mb. Downward motion behind the front is even stronger and reaches 5 μb s^{-1}. The horizontal scale of the vertical transverse circulation is about 500 km. Although this experiment uses an idealized initial field, the structure of the simulated features are qualitatively similar to those observed (Fig. 1b).

After a 36-h integration (1800 LST, the second day, Figs. 4b and 4d), the frontal intensity is further enhanced. The surface horizontal potential temperature gradient increases to 12 K (100 km)$^{-1}$. Major enhancement is confined to below 850 mb. The upward motion over the surface front has increased to -7 μb s^{-1}, indicating that the transverse circulation is also strengthened.

An important feature of the simulated low-level front is that a well-mixed isentropic layer develops above the low-level frontal zone. In the 12-h simulation, it is near 500 mb and has a depth of 100 mb, which is rather shallow. By hour 36, this layer has extended to 300 mb. The maximum radiative heating near the top of the dust (700–600 mb, Fig. 2b) is favorable for the development of this mixed layer. In their study of Saharan dust storm forced by strong surface heating, Prospero and Carlson (1980) found that a deep isentropic mixed layer develops, which favors the transport of the dust to the top of the mixed layer at 500 mb. Our simulation shows that once the dust is carried to the lower troposphere, it is favorable for creating a deep mixed layer in the middle troposphere.

To examine the effect of dust heating, the differences in potential temperature and vertical velocity between experiments DRH and CON are shown in Fig. 5. It can be seen that the surface potential temperature behind the front in DRH is 2 K cooler than that in CON at hour 12 and 6 K cooler at hour 36. Ahead of the surface front, the surface potential temperature in DRH is 6 K warmer than that in CON at hour 12 and 8 K warmer at hour 36. The cooling behind and warming ahead of the front below 900 mb in DRH indicate that the differential surface sensible heat flux, which is modified by the dust distribution, contributes to surface frontogenesis.

A sloping belt of pronounced warming occurs in DRH between 900 and 650 mb, above the surface cooling area. The axis of maximum warming, paralleling the front, shows a slope of $1/100$ and locates about 100 km ahead of the low-level front. Obviously, this warming belt contributes to the low-level frontogenesis. It should be noted that this warming belt is quite different from the dust heating area shown in Fig. 3b. The warming is contributed not only by the direct dust heating but also by the nonlinear interaction between the frontal circulation, dust heating, and the surface sensible heat fluxes.

The difference in vertical motion between DRH and CON (Figs. 5a and 5b) is quite similar to the vertical

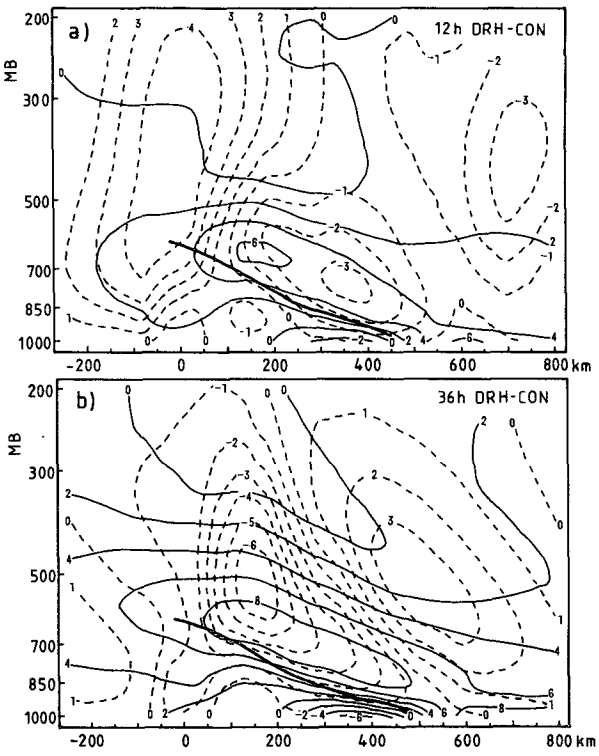

FIG. 5. (a) The difference of potential temperature [solid lines (K)] and vertical motion [dashed lines (μb s^{-1})] between DRH and CON for the 12-h simulation. (b) Same as in (a) but for a 36-h simulation. Thick solid line indicates the maximum potential temperature gradient in the DRH simulation.

velocity in DRH (Figs. 4a and 4b). This indicates that the dust heating has induced a much stronger frontal circulation.

Let the x axis parallel the isentropes; then the two-dimensional frontogenesis equation can be written as (Bluestein 1985)

$$\underset{\mathrm{F}}{\frac{d}{dt}\left|\frac{\partial\theta}{\partial y}\right|} = \left(\underset{\mathrm{F_1}}{-\frac{\partial v}{\partial y}\frac{\partial\theta}{\partial y}} \underset{\mathrm{F_2}}{-\frac{\partial\omega}{\partial y}\frac{\partial\theta}{\partial p}} \underset{\mathrm{F_3}}{+\frac{1}{\pi}\frac{\partial Q}{\partial y}} \right),$$

where v and ω are the horizontal and vertical velocity, Q is the diabatic heating, and $\pi = C_p(p/1000)^{R/C_p}$. The terms of F_1 and F_2 on the right-hand side represent the frontogenesis forcing due to horizontal confluence (diffluence) and vertical twisting, respectively. The third term F_3 is the contribution of diabatic heating on frontogenesis. Figures 6a–d depict the difference of frontogenetic forcing of F_1, F_2, F_3, and total frontogenesis F between the DRH and CON simulations after a 12-h integration. Diabatic frontogenetic forcing (dust radiative heating and surface sensible heat flux) is the dominant term in the low-level frontogenesis (Fig. 6c). The large value of F_3 below 850 mb is the result of differ-

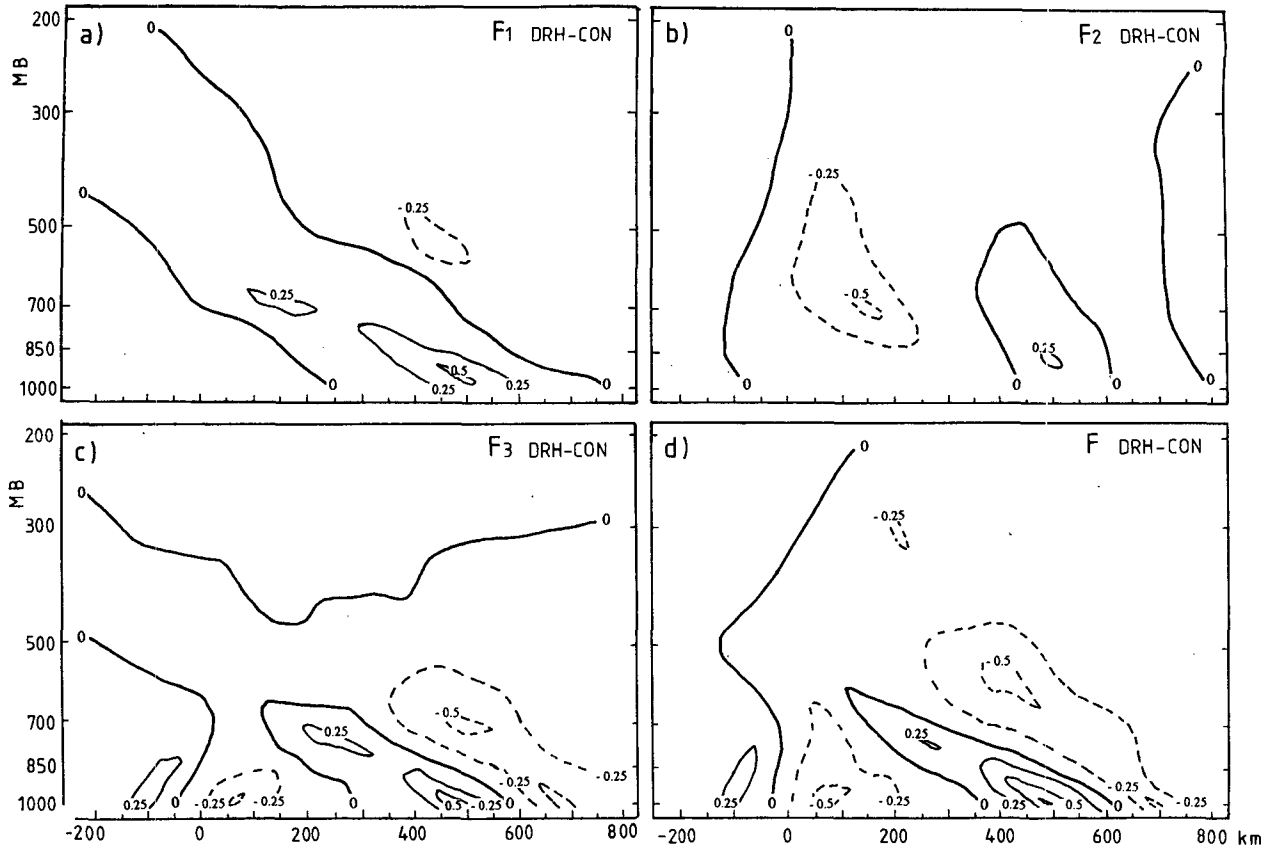

FIG. 6. The differences of two-dimensional frontogenesis forcing between DRH and CON simulations: (a) F_1, horizontal confluence; (b) F_2, vertical twisting; (c) F_3, diabatic heating; and (d) F, total frontogenesis [0.25 K (100 km 3 h)$^{-1}$].

ential surface sensible heat fluxes between dust and clear areas. Another region of strong diabatic frontogenesis between 850 and 600 mb is due to the direct dust radiative heating. Since the dust radiative heating induces a direct vertical circulation along the low-level front (Fig. 4a), the vertical twisting term F_2 leads to frontolysis (Fig. 6b), although the value is small. The positive difference of frontogenesis contributed by horizontal confluence F_1 (Fig. 6a) indicates that the horizontal confluence is much stronger in DRH than that in the CON. The frontogenesis in the DRH simulation is contributed not only by direct diabatic forcing but also by the adiabatic forcing induced by the dust heating. In other words, there is a nonlinear interaction between the dust heating and adiabatic frontogenesis forcing. Consequently, the frontogenesis is greatly intensified and leads to a total forcing F in DRH much larger then that in CON (Fig. 6d). As aforementioned, the intensification of the front in DRH below 850 mb is caused mainly by the differential sensible heat fluxes and the enhancement of confluence, while the frontogenesis between 850 and 600 mb is largely caused by dust radiative heating.

4. Concluding remarks

The results presented here show that the low-level front associated with a dust storm can be significantly intensified by the dust radiative heating. The feedback of dust heating not only warms the atmosphere in the dust region but also enhances the adiabatic baroclinic forcing, leading to stronger low-level frontogenesis. In other words, the dust-related thermal forcing significantly affects the evolution of the dust storm. Including the dust radiative scheme in the model will improve the weather forecasts in the arid and desert areas.

As stated earlier, the dust heating as estimated here represents an upper bound. To obtain a more realistic simulation of the dust effect, further improvement of the radiative scheme is needed. The longwave radiation should be included in the model in order to simulate the diurnal variation in the intensity of the front. Also, the life cycle of the dust, including the vertical and horizontal transport of the dust, should be considered.

Acknowledgments. The authors are very grateful to Drs. Antony Hollingsworth, G.-X. Wu, Eric Smith, and two anonymous reviewers for their valuable comments.

This research is supported by Chinese Natural Science Foundation Grant 49335060.

APPENDIX

The Dust Radiative Heating Scheme

The atmosphere is divided into a sufficient number of layers so that each layer can be considered homogeneous (Fig. A1). Under the two-stream approximation, with the assumption of no internal sources (e.g., thermal emission at long wavelength) the radiative transfer equations in the jth layer for diffused and direct solar radiation can be expressed as (Zdunkowski et al. 1974; Meador and Weaver 1980)

$$\frac{dF^+}{d\tau} = \gamma_1 F^+ - \gamma_2 F^- - S_{j-1}\omega\beta_0 \exp(-\tau/\mu_0) \quad \text{(A1)}$$

$$\frac{dF^-}{d\tau} = \gamma_2 F^+ - \gamma_1 F^- - S_{j-1}\omega(1-\beta_0)\exp(-\tau/\mu_0) \quad \text{(A2)}$$

$$\frac{dS}{d\tau} = -\frac{S}{\mu_0}, \quad \text{(A3)}$$

where F^+ and F^- are the upward and downward diffused flux induced by *direct* solar radiation S_{j-1} at the top of the jth layer; τ is the optical depth, which is the extinction coefficient integrated with respect to height from the top of the layer; ω is the single scattering albedo; β_0 is the ratio of backward scattering to the total scattering; μ_0 is the ordinate of the sun; $\mu_0 = \cos\theta_Z$, θ_Z is the solar zenith angle; and γ_1 and γ_2 are the coefficients, which can be determined with appropriate approximation.

Using a hybrid modified Eddington–delta function, Meador and Weaver (1980) obtained the expressions for γ_1 and γ_2 as

$$\gamma_1 = \frac{7 - 3g^2 - \omega(4 + 3g) + \omega g^2(4\beta_0 + 3g)}{4[1 - g^2(1 - \mu_0)]} \quad \text{(A4)}$$

$$\gamma_2 = \frac{1 - g^2 - \omega(4 - 3g) - \omega g^2(4\beta_0 + 3g - 4)}{4[1 - g^2(1 - \mu_0)]}. \quad \text{(A5)}$$

Here g is the asymmetry factor parameter. Their numerical results showed that this approximation has accuracy comparable to other two-stream approximation models.

Consider a homogeneous layer $(j-1, j)$ with an optic depth τ_j; the coefficients ω, β_0, γ_1, and γ_2 are assumed to be constant in this layer. Equations (A1)–(A3) can be integrated analytically across this layer. We have

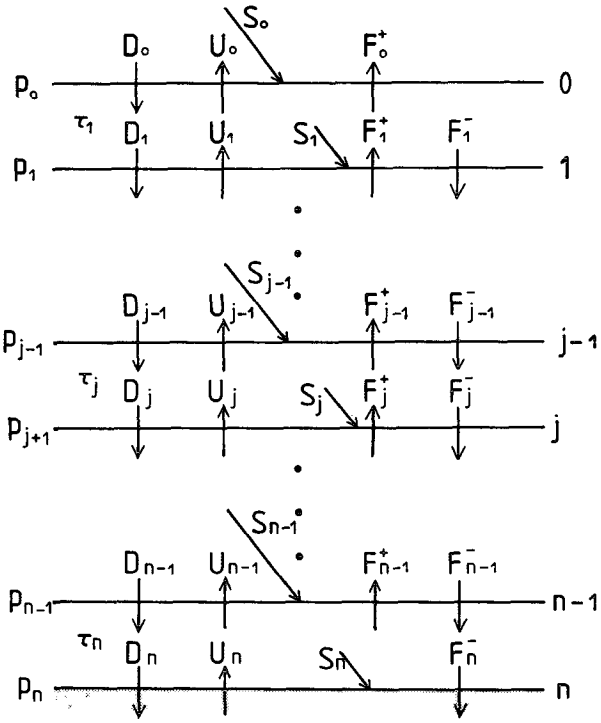

FIG. A1. Calculation of the multiple radiative flux. See appendix for explanation.

$$S_j = S_{j-1}\exp(-\tau_j/\mu_0) = S_0 \exp\left(-\sum_{j=1}^{j}\tau_j/\mu_0\right) \quad \text{(A6)}$$

and

$$F_{j-1}^+ = R_j' \mu_0 S_{j-1} \quad \text{(A7)}$$

$$F_j^- = T_j' \mu_0 S_{j-1}. \quad \text{(A8)}$$

For the jth layer, $\exp(-\tau_j/\mu_0)$ is the parallel transmittance for the direct solar radiation, R_j' is the diffused reflectance, and T_j' is the diffused transmittance of the *direct* solar radiation. Here S_0 is the solar irradiance at the top of the atmosphere. From Meador and Weaver (1980),

$$R_j' = \frac{\omega}{B} \times [(1 - k\mu_0)(\alpha_2 + k\beta_0)\exp(k\tau_j) - (1 + k\mu_0)(\alpha_2 - k\beta_0)\exp(-k\tau_j) - 2k(\beta_0 - \alpha_2\mu_0)\exp(-\tau_j/\mu_0)] \quad \text{(A9)}$$

$$T_j' = \frac{\omega \exp(-\tau_j/\mu_0)}{B} \times [(1 - k\mu_0)(\alpha_1 - k + k\beta_0) \times \exp(-k\tau_j) - (1 + k\mu_0)(\alpha_1 + k - k\beta_0) \times \exp(k\tau_j) + 2k(1 - \beta_0 + \alpha_1\mu_0)\exp(\tau_j/\mu_0)], \quad \text{(A10)}$$

where

$$k = (\gamma_1^2 - \gamma_2^2)^{1/2},$$

$$\alpha_1 = \gamma_1 - \gamma_1\beta_0 + \gamma_2\beta_0, \quad \alpha_2 = \gamma_2 + \gamma_1\beta_0 - \gamma_2\beta_0,$$

$$B = (1 - k^2\mu_0^2)[(k + \gamma_1)\exp(k\tau_j) + (k - \tau_1)\exp(-k\tau_j).$$

Following Geleyn and Hollingsworth (1979), the multiple scattering radiative transfer equation can be written as (Fig. A1)

$$\begin{aligned} U_0 &= R_1D_0 + T_1U_1 + F_0^+ \\ D_1 &= T_1D_0 + R_1U_1 + F_1^- \\ U_1 &= R_2D_1 + T_2U_2 + F_1^+ \\ D_j &= T_jD_{j-1} + R_jU_j + F_j^- \\ U_j &= R_{j+1}D_j + T_{j+1}U_{j+1} + F_j^+ \\ U_{n-1} &= R_nD_{n-1} + T_nU_n + F_{n-1}^+ \\ D_n &= T_nD_{n-1} + R_nU_n + F_n^-. \end{aligned} \tag{A11}$$

Here F_{j-1}^+ and F_j^- are calculated from (A7)–(A8); U_j and D_j represent the total upward and downward diffused solar flux, which include the source function F_{j-1}^+, F_j^-, and diffused solar flux transmitted or reflected from other layers; R_j and T_j are the diffused reflectance and diffused transmittance of the *diffused* solar radiation incident to the layer, which can be solved from (A1) and (A2) with the direct solar radiation term S_{j-1} omitted (Meador and Weaver 1980):

$$R_j = \gamma_2[1 - \exp(-2k\tau_j)]/H \tag{A12}$$

$$T_j = 2k\exp(-2k\tau_j)/H, \tag{A13}$$

where

$$H = k + \gamma_1 + (k - \gamma_1)\exp(-2k\tau_j).$$

Here U_j and D_j can be solved from Eq. (A11) with the boundary conditions $D_0 = 0$ and $U_n = \alpha[D_n + S_0\mu_0 \times \exp(\Sigma_{j=1}^n \tau_j/\mu_0)]$, where α is the surface albedo.

The number of dust particles is expressed by the extinction coefficient at wavelength 0.55 μm. The size spectrum and the real and imaginary indices of refraction for the Asian desert dust are not available; thus the Carlson and Benjamin (1980) model for the Saharan dust is used. The mean cross section of absorption and scattering σ_a, σ_S, and the parameters g, ω, and β_0 in (A8) and (A9) are calculated by a program for Mie scattering (Bohren and Huffman 1983).

The solar spectrum is divided into 26 wave bands (from 0.2 to 4.3 μm). For each wave band the effective solar irradiance E_j at level j is

$$E_j = D_j - U_j + \mu_0 S_j.$$

The radiative heating Q_R is the summation over the whole solar spectrum:

$$Q_R = \sum (E_{j-1} - E_j)/(p_{j-1} - p_j), \tag{A14}$$

where p_{j-1} and p_j are the pressures at the $j-1$ and j level, respectively.

REFERENCES

Anthes, R. A., and T. T. Warner, 1978: Development of hydrodynamic models suitable for air pollution and mesometeorological studies. *Mon. Wea. Rev.*, **106,** 1045–1078.

Arakawa, A., and V. R. Lamb, 1981: A potential entrophy and energy conserving scheme for the shallow water equations. *Mon. Wea. Rev.*, **109,** 18–36.

Bluestein, H. B., 1985: Fronts and jet streaks: A theoretical perspective. *Mesoscale Meteorology and Forecasting,* P. S. Ray, Ed., Amer. Meteor. Soc., 173–215.

Bohren, C. F., and D. R. Huffman, 1983: Absorption and scattering of light by small particles. John Wiley & Sons, 530 pp.

Carlson, T. N., and S. G. Benjamin, 1980: Radiative heating for Saharan dust. *J. Atmos. Sci.*, **137,** 193–213.

Chen, T.-J., and H.-J. Chen, 1987: Study on large-scale features of dust storm system in East Asia. *Pap. Meteor. Res.*, **10,** 57–80.

Duce, R., C. K. Unni, B. Ray, J. M. Prospero, and J. Merrill, 1980: Long range transport of soil atmospheric dust from Asia to the tropical North Pacific. *Science,* **209,** 1522–1524.

Geleyn, J. F., and A. Hollingsworth, 1979: An economical method for the computation of the interaction between scattering and line absorption of radiation. *Beitr. Phys. Atmos.*, **52,** 1–16.

Hack, J. J., and W. H. Schubert, 1981: Lateral boundary condition for the tropical cyclone model. *Mon. Wea. Rev.*, **109,** 1404–1420.

Meador, W. E., and W. R. Weaver, 1980: Two-stream approximations to radiative transfer in planetary atmospheres. *J. Atmos. Sci.*, **37,** 630–643.

Prospero, J. M., and T. N. Carlson, 1980: Saharan air outbreaks over the tropical North Atlantic. *Pure Appl. Geophys.*, **119,** 677–699.

Qiu, J.-H., Y.-Z. Zhao, and H.-Q. Wang, 1984: Detection of aerosol extinction coefficient profiles during dust storms by lidar (in Chinese). *Atmos. Sci.*, **8,** 205–210.

Shaw, G. E., 1980: Transport of Asian desert aerosol to the Hawaiian islands. *J. Appl. Meteor.*, **19,** 1254–1259.

Suarez, M. J., and A. Arakawa, 1979: Description and preliminary results of the nine-level UCLA general circulation model. Preprints, *Fourth Conf. on Numerical Weather Prediction,* Silver Spring, MD, Amer. Meteor. Soc., 290–297.

Xu, G.-C., M.-L. Chen, and G.-X. Wu, 1979: On an extraordinary heavy sandstorm on 22 April 1977 in Gansu (in Chinese). *Acta Meteor. Sin.*, **37,** 26–35.

Zdunkowski, W. G., G. J. Korb, and C. T. Davis, 1974: Radiative transfer in model clouds of variable and height constant liquid water content as computed by approximate and exact methods. *Beitr. Phys. Atmos.*, **47,** 157–186.